Shear-induced crystallization of an amorphous system

Anatolii V. Mokshin and Jean-Louis Barrat
Université de Lyon; Univ. Lyon I, Laboratoire de Physique de la Matière Condensée et des Nanostructures; CNRS, UMR 5586, 43 Bvd. du 11 Nov. 1918, 69622 Villeurbanne Cedex, France
(Received 21 November 2007; revised manuscript received 28 January 2008; published 29 February 2008)

The influence of a stationary shear flow on the crystallization in a glassy system is studied by means of molecular dynamics simulations and subsequent cluster analysis. The results reveal two opposite effects of the shear flow on the processes of topological ordering in the system. Shear promotes the formation of separated crystallites and suppresses the appearance of the large clusters. The shear-induced ordering proceeds in two stages, where the first stage is related mainly to the growth of crystallites and the second stage is due to an adjustment of the created clusters and a progressive alignment of their lattice directions. The influence of strain and shear rate on the crystallization is also investigated. In particular, we find two plausible phenomenological relations between the shear rate and the characteristic time scale needed for ordering of the amorphous system under shear.

DOI: 10.1103/PhysRevE.77.021505 PACS number(s): 46.35.+z, 05.70.Ln, 83.50.−v

I. INTRODUCTION

Most liquids, under cooling, undergo a first order transition to a crystalline phase. The classical view is that this transition takes place through a homogeneous nucleation process and can be reasonably well described in the framework of classical nucleation theory [1–6]. Nucleation theory is based on the fact that a nucleation event is an activated process, taking place on time scales much larger than the characteristic time scale of the microscopic dynamics. The free energy of forming crystalline embryos from the metastable surroundings is defined by a positive surface and negative bulk contributions. The surface term corresponds to the cost in free energy for creation of an interface between parent and incipient (say, crystalline) phases, whereas the bulk term is proportional to the volume of the nucleus. The crystal size, wherein the free energy reaches a maximum and the system begins to crystallize, defines the critical nucleus.

With the increase of the degree of supercooling ΔT the description of the transition toward the ordered phase becomes more complicated. On the one hand, the height of nucleation barrier decreases with supercooling ΔT as $1/\Delta T^2$, so that at supercooling $\sim$40% and higher a very fast crystal nucleation could be expected [7]. On the other hand, observations at a very large supercooling indicate nascent droplets that exhibit a ramified structure [8] and a crystallization process with a more extended, collective, and spatially scattered character that may be attributed to a spinodal regime [9]. Such tendencies are, however, balanced by the kinetic slowing down, which makes the ordering process more and more difficult to observe as the temperature is lowered. In the limit, where the system is deeply supercooled and becomes glassy, crystal formation is completely unobservable on experimental time scales.

The application of external field on a glassy material may change considerably this picture of nucleation. What influence has an external forcing, such as shear flow and/or strain, on the nucleation process of a glass? Experimental studies of amorphous (co)polymers reveal the appearance of shear-induced crystallization [10–13]. This is verified by molecular dynamics simulations, which provide some evidence for an increase of ordering in sheared polymeric and model binary glasses [14,15]. Recently, results of molecular dynamics simulations showed that the *oscillating shear strain* can promote crystallization in model jammed systems [16]. However, the influence of shear rate and strain on the ordering processes as well as the possibility of crystallization under stationary shear have remained unclear.

At a moderate supercooling, simulation results on the sheared colloidal melts of Refs. [17,18] demonstrate the suppression of nucleation by a homogeneous shear flow. More precisely, they reveal that the probability of the nucleation decreases, while the size of critical nuclei increases with the shear rate. In glassy systems at low temperatures, on the other hand, it is reasonable to suggest that the external drive can *activate* dynamical processes [19,20]. A moderate external shear field will increase the local diffusivity in the system, hence having a positive influence on the kinetic factors for nucleation, and thereby it will trigger crystallization. However, a continued shear may destroy crystalline nuclei as they form and a steady nonequilibrium state can be expected.

In the present work we focus on the influence of a *stationary shear* on the ordering processes in a glassy system. In Sec. II we describe our model system and the analysis used to identify crystallinity and solidlike clusters. The simulation results and outcomes of cluster analysis are shown in Sec. III, where we also study the influence of strain and shear rate on the ordering. We finish in Sec. IV with a discussion of the main results.

II. SYSTEM AND PROCEDURES

Our system consists of 23 328 particles interacting through a standard truncated and shifted Lennard-Jones potential

$$U(r)=\begin{cases}4\epsilon\left[\left(\dfrac{\sigma}{r}\right)^{12}-\left(\dfrac{\sigma}{r}\right)^{6}-\left(\dfrac{\sigma}{r_c}\right)^{12}+\left(\dfrac{\sigma}{r_c}\right)^{6}\right], & r\le r_c,\\ 0, & r>r_c.\end{cases} \tag{1}$$

ϵ and σ are the characteristic energy and length scales and $r_c=2.5\sigma$ is the cutoff distance. The following reduced units

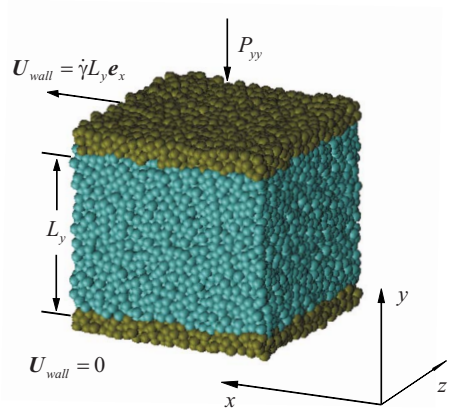

FIG. 1. (Color online) Snapshot of the simulation cell. Two parallel amorphous walls (dark particles) restrict the sheared system. The particles of the top wall are removed with the velocity proportional to the distance between the walls L_y, which is variable with the time due to the normal pressure P_{yy}. The particles of the bottom wall are fixed.

are used in this work. The time is in units of $\tau = \sigma\sqrt{m/\epsilon}$, where the mass m is set to unity. All distances are given in units of σ. The temperature is in units of ϵ/k_B, whereas the pressure and the stress are in units of ϵ/σ^3. The time step $\Delta\tau$ used in our simulations is 0.005τ.

We start with a system equilibrated in the liquid state at the temperature $T=1.65\epsilon/k_B$ in a cubic simulation box ($V=L^3$ and $L=30.2327\sigma$) with periodic boundary conditions in all directions. After this, the system is quenched to the temperature $T=0.15\epsilon/k_B$ within a time interval $t=2.5\tau$. In the case of argon atoms with the Lennard-Jones parameters $\epsilon/k_B=120$ K and $\sigma=3.4$ Å this corresponds to a cooling rate $\sim 10^{13}$ K/s [21]. After such a rapid quench, the system at this temperature is in a glassy state [22–25]. This is evidenced by the zero slope of mean square displacement on the time scale of our simulations, which is a signature of "structural arrest." The disordered character of the structure is also evident from the split second peak of the pair distribution function, typical of an amorphous material.

Before shearing, the system is allowed to "age" during $t=10\,000\ \tau$ without any external forcing. In order to shear the system, we create two parallel solid walls by freezing all the particles in the x-z plane over the range of three interparticle distances from both ends of the simulation box in the y direction. Both walls are amorphous. By using walls, we can impose an average strain rate without any assumptions about the resulting flow inside of the sample. A snapshot of the simulation cell is presented in Fig. 1. Twelve independent samples were prepared with the same procedure.

A constant shear rate $\dot{\gamma}$ is then applied by moving in the x direction all the atoms of the top wall with the instantaneous velocity

$$\boldsymbol{U}_{\text{wall}} = \dot{\gamma} L_y \boldsymbol{e}_x, \tag{2}$$

whereas the particles of the bottom wall remain fixed; L_y is the distance between the walls. Periodic boundary conditions are applied along the x and z directions only. All the results are for a constant normal pressure $P_{yy}=1.1867\epsilon/\sigma^3$ (corresponding to the pressure observed initially). Temperature is controlled by rescaling of the velocity component of the particles along the neutral z direction, which is perpendicular to the shear x and the velocity gradient y directions.

In order to identify the local structure and, in particular, the appearance of solidlike clusters, we use the local order analysis introduced originally in the work of Steinhardt *et al.* [26] and developed by Frenkel and co-workers [7,27,28]. An important advantage of this method is that (i) it allows one to recognize the crystallinity regardless of a specific structure and (ii) the crucial parameters here, such as local and global order parameters, are rotationally invariant, so that the orientation of clusters in space is irrelevant.

First of all, the local surroundings of each atom can be characterized by a $(2\times 6+1)$-dimensional complex vector with the following components:

$$q_{6m}(i) = \frac{1}{N_b(i)} \sum_{j=1}^{N_b(i)} Y_{6m}(\theta_{ij}, \varphi_{ij}), \tag{3}$$

where $Y_{6m}(\theta_{ij}, \varphi_{ij})$ are the spherical harmonics and $N_b(i)$ denotes the number of the nearest neighbors of particle i; θ_{ij} and φ_{ij} are the polar and azimuthal angles formed by the radius-vector $\mathbf{r}_{ij}$ and some reference system. We define "neighbors" as all atoms located within a given radius $r_c=1.5\sigma$ around an atom i, i.e., $|\mathbf{r}_{ij}|<r_c$, where r_c corresponds practically to the first minimum in the pair distribution function. The local orientational order parameter can be defined for each atom i as

$$q_6(i) = \left(\frac{4\pi}{13} \sum_{m=-6}^{6} |q_{6m}(i)|^2 \right)^{1/2}, \tag{4}$$

which is rotationally invariant. Thus the global orientational order parameter can be defined as an average of $q_{6m}(i)$ over all N particles:

$$\mathcal{Q}_6 = \left(\frac{4\pi}{13} \sum_{m=-6}^{6} \left| \frac{\sum_{i=1}^{N} \sum_{j=1}^{N_b(i)} Y_{6m}(\theta_{ij}, \varphi_{ij})}{\sum_{i=1}^{N} N_b(i)} \right|^2 \right)^{1/2}. \tag{5}$$

For perfect fcc, bcc, and hcp systems one has $\mathcal{Q}_6=0.5745$, $\mathcal{Q}_6=0.5106$, and $\mathcal{Q}_6=0.4848$, respectively, whereas in a fully disordered system in the limit of large sizes (e.g., a liquid), $\mathcal{Q}_6$ is close to zero [29]. Hence an increase of this quantity provides the evidence for the formation of local crystallites. To estimate the degree of ordering (crystallinity) in our system we use, along with $\mathcal{Q}_6$, the potential energy as well as the number of "solidlike" particles.

The occurrence of ordered structures can also be observed in the behavior of the radial distribution function. However, this function corresponds to the averaged result for the whole system, and, as a consequence of this, can be insensitive to the appearance of a few local clusters.

For the study of local structures we apply the following cluster analysis [7]. For every pair of nearest neighbors, say i and j, the following condition is considered:

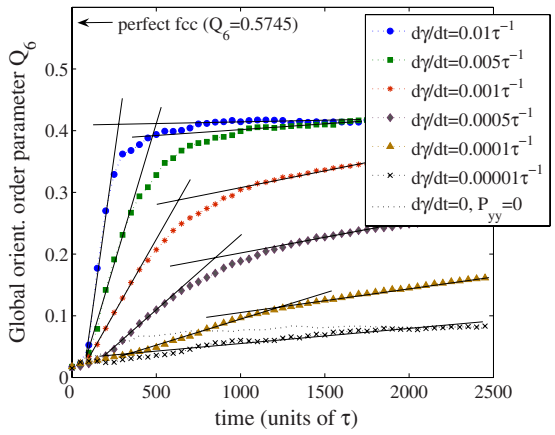

FIG. 2. (Color online) Evolution of the global orientational order parameter $\mathcal{Q}_6$ at the various shear rates $\dot{\gamma}$ as a function of time. The shear rate increases from bottom to top. The full lines are linear fits to the data. The arrow indicates the value of $\mathcal{Q}_6$ for a perfect fcc structure.

$$\left| \sum_{m=-6}^{6} \tilde{q}_{6m}(i)\tilde{q}^{*}_{6m}(j) \right| > 0.5, \tag{6}$$

where $\tilde{q}_{6m}(i)$ is the complex vector $q_{6m}(i)$ defined by Eq. (3) and normalized in accordance with

$$\sum_{m=-6}^{6} \tilde{q}_{6m}(i)\tilde{q}^{*}_{6m}(i) = 1. \tag{7}$$

Condition (6) allows one to verify that atom j belongs to an ordered structure around atom i. If atom i has seven or more *neighbors* satisfying the condition (6), then this atom is considered as solid-like, i.e., it is included in an ordered crystalline structure.

III. RESULTS

We now turn to the results, which quantify the effect of shear on an initially amorphous sample. The time evolution of the global orientational order parameter $\mathcal{Q}_6$ for various values of the shear rate $\dot{\gamma}$ is shown in Fig. 2. Note that the results presented here have been averaged over different runs. From these results, it appears clearly that the degree of order in the system is enhanced by shear. Moreover, at the larger values of the shear rate $\dot{\gamma}$ the ordering takes place rather rapidly; $\mathcal{Q}_6$ levels off after this initial transient. For $\dot{\gamma}=0.01$ and $0.005\tau^{-1}$ the order parameter reaches a plateau value with $\mathcal{Q}_6 \approx 0.42$ over the time scale of observation. At lower values of $\dot{\gamma}$ *the rate of ordering* (defined as the time derivative of the order parameter) is lower and decreases with the time, as is clearly seen from the change in slope in the curves shown in Fig. 2. As a result, the time window $t=2500\tau$ presented in Fig. 2 is not sufficient to achieve a maximal ordering at slow shear rates. It is particularly noteworthy that the shear can initially prevent the formation of small clusters, which would appear even in the absence of shear. This weak suppression effect is observed for very small shear rates $\dot{\gamma}=0.0001$ and $0.000\,01\ \tau^{-1}$, where the values of $\mathcal{Q}_6$ are lower in comparison with the case of a sample at rest. Nevertheless, the increase of the order parameter with time is clearly detected even for these small shear rates. Our first conclusion is therefore that shear enhances crystallinity with a rate which depends on the shear rate.

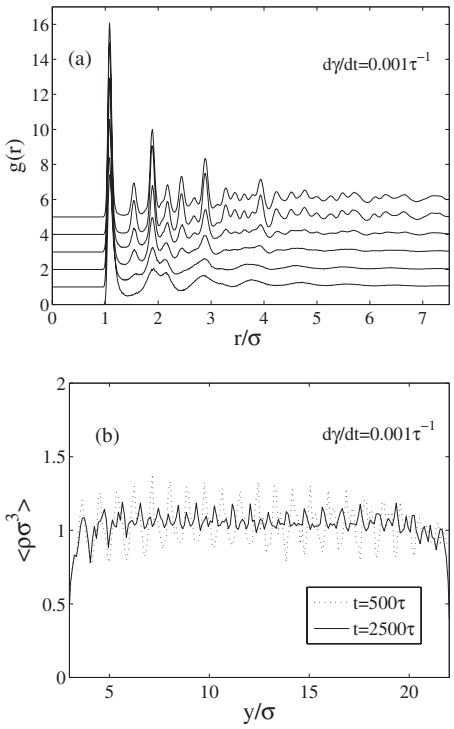

FIG. 3. Structural characteristics of the sample under shear (at the shear rate $\dot{\gamma}=0.001\tau^{-1}$). (a) Radial distribution function at the different times after starting the shear flow: $t=0$, 250, 500, 750, 1500, and 2500τ (from bottom to top). The curves are shifted upward for clarity. (b) Density profiles for two different times as averaged over a time window of 10τ.

Although the largest value of the order parameter $\mathcal{Q}_6$ obtained by shearing the glass is low in comparison with $\mathcal{Q}_6$ of a perfect fcc structure, it indicates a high level of crystallinity in the system. The formation of crystalline ordered structures in a sample can also be observed from the radial distribution function as shown in Fig. 3(a) for a particular shear rate $\dot{\gamma}=0.001$ and different times after starting up of the shear. In the first three curves the appearance of crystalline structures is evident from the rise of the extra peak between the first and second maxima in the distribution, which is a typical signature of fcc structures. The pair correlation function calculated at large times shows that the order extends over large distances, with oscillations extending up to $r>4\sigma$. Such a long-range ordering could also be associated with layering of the system under shear. To check this, we evaluated the density profiles at different times as a function of the distance from the walls. As can be seen in Fig. 3(b), which presents the density profiles at $t=500$ and 2500τ [the curves for intermediate times are very similar to those presented in Fig. 3(b)], the transverse order is present, but not particularly pronounced.

Moreover, the layering is weaker for $t=2500\tau$, whereas the pair correlation function displays the more pronounced

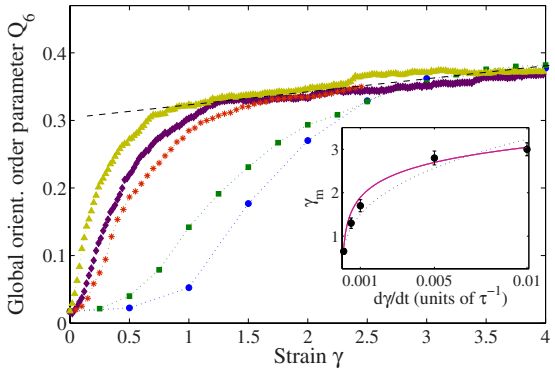

FIG. 4. (Color online) Main: Strain dependence of the global orientational order parameter $\mathcal{Q}_6$ at the different shear rates $\dot{\gamma}=0.0001$, 0.0005, 0.001, 0.005, and $0.01\tau^{-1}$ (from left to right). The correspondence between curves and shear rates is the same as in Fig. 2. The dashed line is the linear interpolation, indicating the steady behavior (plateau) in the strain dependence of order parameter. Inset: Shear rate dependence of the strain γ_m, at which the order parameter reaches the plateau value. Errors are defined by the change of slope in $\mathcal{Q}_6(\gamma)$. The solid and dotted curves are the logarithmic and power-law approximations, respectively (see text).

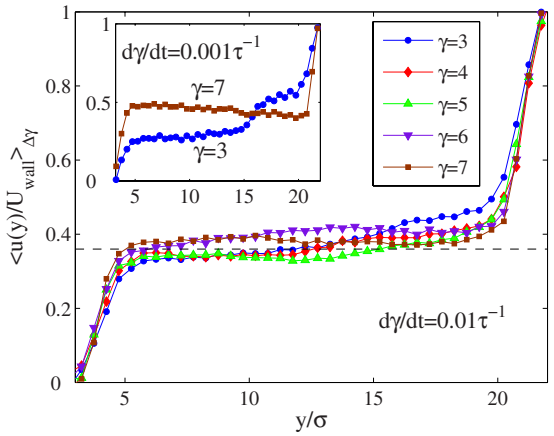

FIG. 5. (Color online) Rescaled velocity profile as a function of distance from the bottom (unmoved) wall. Main: Shear with $\dot{\gamma}=U_{\text{wall}}/L_y=0.01\tau^{-1}$ at different points of the strain γ above $\gamma_m=3$. The broken line corresponds to $u/U_{\text{wall}}=0.36$. Inset: Shear rate $\dot{\gamma}=0.001\tau^{-1}$ at two different strains above γ_m. Results are averaged over the time window $t=\Delta\gamma/\dot{\gamma}$, where $\Delta\gamma=0.01$ is the strain scale. All runs exhibit a similar behavior.

structure. This observation leads to the conclusion that the long-range order observed in the pair correlations is caused mainly by the formation of a crystalline cluster.

A. Strain and strain rate dependence

The strain dependence of the global order parameter $\mathcal{Q}_6$ is shown in Fig. 4. It can be seen that the order parameter increases with the strain γ for all values of the shear rate. Moreover, the evolution of the order parameter with strain is clearly separated into two steps. The first stage, during which the order parameter rises rapidly, is shear rate dependent. After this fast increase, $\mathcal{Q}_6$ reaches a "universal" (shear rate independent) behavior shown by a straight dashed line in Fig. 4. At this stage, the order parameter demonstrates a very slow increase and eventually levels off at large strains.

In order to quantify the influence of shear rate on the ordering, we introduce the "ordering strain" γ_m. This quantity defines the strain scale, where the evolution of $\mathcal{Q}_6$ merges with the universal behavior shown by a dashed line in Fig. 4. The shear rate dependence of γ_m is plotted in the inset of Fig. 4. The data for $\gamma_m(\dot{\gamma})$ can be fitted either by a power law or by a logarithmic dependency on the strain rate:

$$\gamma_m \propto \dot{\gamma}^{1+n}, \quad n=-2/3, \tag{8a}$$

$$\gamma_m = \gamma_0 + \frac{1}{2}\ln(\dot{\gamma}), \quad \gamma_0 = \text{const}. \tag{8b}$$

It should be noted that the power law behavior is supported by the idea that the typical relaxation time t_α of a sheared glassy system decreases with the strain rate as $\dot{\gamma}^{-2/3}$ (see Ref. [30]). Assuming that a similar dependency holds in our crystallizing system and the initial rise of $\mathcal{Q}_6$ corresponds to a typical relaxation time, we obtain

$$t_m \sim \dot{\gamma}^{-2/3}, \tag{9}$$

where $t_m=\gamma_m/\dot{\gamma}$. Such a power-law decay of the crystallization time with the shear rate could also be related to the one found experimentally in Refs. [11,13].

Although the possible relation between the characteristic time scale t_α and the time of ordering t_m under shear is attractive [30], it is seen in the inset of Fig. 4 that the power law with Eq. (8a) does not provide a perfect fit of γ_m at shear rates $\dot{\gamma}\approx 0.01\tau^{-1}$ and higher, whereas the logarithmic dependence (8b) gives a good fit to the data for all values of the shear rate.

We finally discuss our results with regard to recent observations reported by Duff and Lacks [16]. These authors studied the ordering of a similar system under an *oscillatory* strain in the low temperature and low shear rate limit. A degree of ordering comparable to the one observed in our study was obtained after two cycles with the amplitude 0.25. As a result, it would correspond to a total strain $\gamma_m=0.5$, which is comparable to the values obtained by us at the lowest shear rates.

B. Nature of the semicrystalline state

Although the system clearly becomes more ordered under the influence of strain, the degree of order achieved by our system is low in comparison to that of a perfect crystal. A very remarkable fact is that, at large strains, the order parameter $\mathcal{Q}_6$ appears to be dependent only on strain and not on strain rate. This observation indicates some "universality" of the semicrystalline state created in the system. This observation is, however, easily explained by considering the velocity profiles in the sheared systems. The velocity profiles presented in Fig. 5 exhibit a strong localization of the shear in two shear bands located near the solid walls. The semicrystalline part of the sample, on the contrary, flows with an

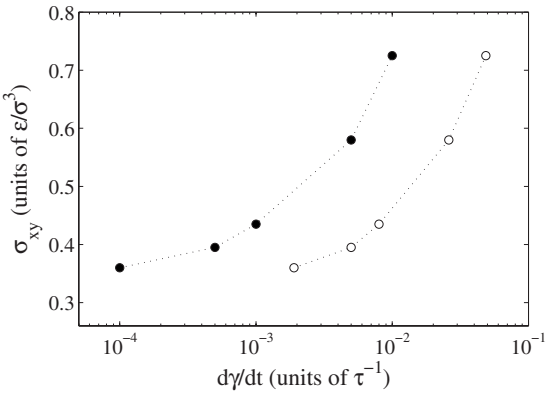

FIG. 6. Connected empty circles: Shear stress vs strain rate in the sheared part of the velocity profiles shown in Fig. 5. Connected full circles: Stress as a function of the average shear rate in the sample. These curves are indicative of a coexistence between a rapidly flowing shear band and a nonflowing solid below its yield stress.

almost uniform velocity (although some plastic activity is also taking place in this "nonflowing" part). The situation described here is very similar to the shear localization observed in a flowing glass by Varnik *et al.* [31]. The nanocrystalline solid is submitted to a stress, which is insufficient to cause flow, while two strongly fluidized bands sustain the shear entirely. What is remarkable here is the high value of the shear rate and the stress at which this coexistence is observed (see Fig. 6). While the yield of the solid in Ref. [31] was observed for a strain rate slightly above $0.001\tau^{-1}$ and a stress of $0.6\epsilon/\sigma^3$, our results indicate here a yield stress $\sigma_Y > 0.8\epsilon/\sigma^3$.

We expect that this nanocrystalline state consists of an assembly of crystallites with disordered orientations. This set of crystallites can be quantitatively described by means of the cluster analysis presented in Sec. II. The results of this analysis are shown in Fig. 7 as a function of the strain γ for a particular shear rate, since the results for other values of the shear rate are very similar. The sample is imperfectly crystallized in such a way that only ~80% of the particles are involved in crystalline clusters. Obviously, the rapid buildup of crystalline order between $\gamma=0$ and γ_m corresponds to a rapid decrease in the potential energy [see Fig. 7(a)]. The next interesting feature is that the number of solidlike clusters [see Fig. 7(b)], after a significant growth with the strain, remains essentially constant, whereas the evolution of the potential energy and of the order parameter indicates a continued ordering process in the system. This leads to the conclusion that the system under shear decomposes rapidly into a set of crystalline "grains." The subsequent evolution consists of rearrangements involving the grinding of grain boundaries and the alignment of neighboring grains without any significant coarsening.

Another interesting information about the final state of the system can be extracted from the size distribution of the crystalline grains, which is presented in Fig. 8 at three different shear rates. As can be seen from these histograms, the distribution is dominated by small grains involving less than 50 particles. At first sight, the distribution appears to be,

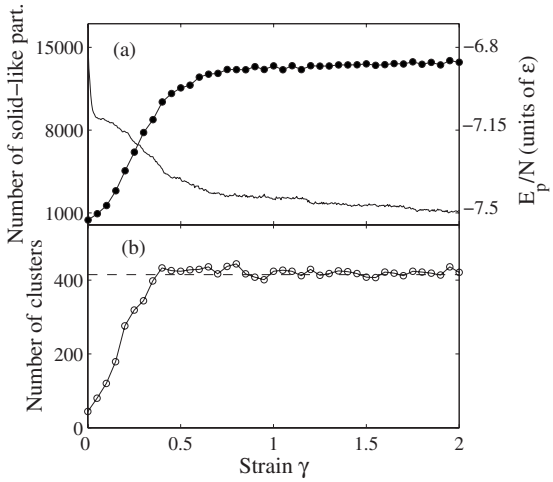

FIG. 7. Different characteristics vs strain at the shear rate $\dot{\gamma}=0.001\tau^{-1}$ after a single run: (a) Number of solidlike particles in a whole system (connected full circles) and potential energy per particle (solid line). (b) Number of crystallites (connected open circles). The dashed line corresponds to the value 415.

within the accuracy of our data, shear rate independent. This is consistent with the universal behavior of the order parameter observed in Fig. 4. Nevertheless, the distribution displays a relatively slow decaying tail for cluster sizes larger than 100 particles. This decay can be well approximated by a power law (see inset of Fig. 8). Closer examination reveals that the weight of this tail depends weakly on shear rate and that larger clusters can be observed at lower shear rates. Unfortunately, the small number of large clusters makes a systematic investigation of this effect difficult.

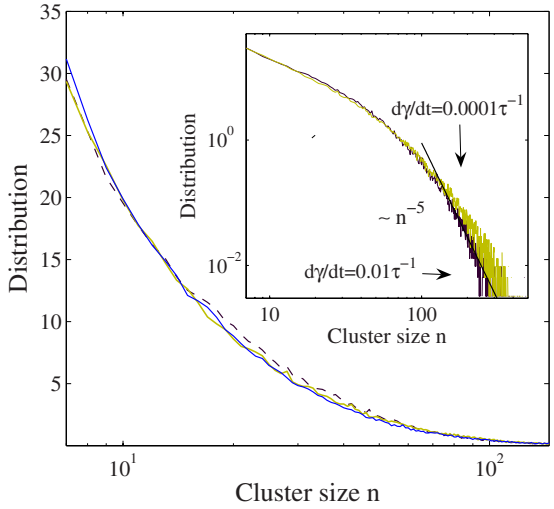

FIG. 8. (Color online) Main: Cluster size distribution at the different shear rates $\dot{\gamma}=0.01$, 0.001, and $0.0001\tau^{-1}$ (dashed, thin, and thick lines, respectively) and for a strain of 400%, where the system is characterized by the order parameter $Q_6 \approx 0.37$ for all shear rates (see Fig. 4). Each histogram is averaged over different runs. Inset: The same distribution in log-log representation. The solid line is the interpolation of the tail of the distribution at $\dot{\gamma}=0.01\tau^{-1}$ by a power-law dependence.

IV. DISCUSSION: SHEAR SUPPRESSION VERSUS SHEAR ENHANCEMENT

Our results demonstrate clearly that the shear increases initially the tendency of a one-component amorphous system toward crystalline order. This behavior should be discussed in the context of the recent studies by Blaak and Löwen, who demonstrated on the contrary a shear suppression of the nucleation rate at moderate undercooling [17], and of the recent results of Ref. [9] concerning the evolution of the nucleation barrier with temperature. Clearly, the main influence of shear at low temperature will be on the kinetic, rather than on the thermodynamic, aspects of the transition. In the absence of shear, the diffusivity is essentially zero, so that the system does not evolve with time. However, according to the classical nucleation picture, one would expect the appearance of crystallinity in the form of a few isolated nuclei after a significant time lag associated with the free energy barrier. Our results, on the contrary, indicate an instantaneous increase of crystalline order as soon as the shear is started that is more consistent with a spinodal description. The system is rapidly driven toward a new energy minimum as soon as a mobility is reinstalled by the shear flow. The order appears uniformly inside the system, which relaxes locally toward a crystalline structure on a time scale, which is characteristic of a sheared glass.

After this initial relaxation, a much slower stage of defect and grain boundary annealing takes place. During this second stage, the state of the system appears to be independent on the strain rate and is determined by the amount of strain only. The system consists of two rapidly flowing sheared bands, separated by a slab of a nanocrystalline solid, which undergoes a very progressive evolution through plastic rearrangements. This nanocrystalline solid appears to have a high yield stress in comparison with a similar Lennard-Jones glass.

It is remarkable that, although the flow rate at the boundary increases, the evolution of the solid slab seems to be insensitive to this flow rate. A possible explanation is in the fact that the energy in a yield stress system is dissipated by the flow, which will serve to activate annealing processes in the solid slab. As a result, the local structural transformations are defined essentially by deformations and insensitive to strain rate.

The nonflowing part of the system can be mainly described as a collection of the crystalline grains of relatively small size. The stationarity in the number of crystallites indicates that the disruption of crystalline order by the shear at the boundaries compensates completely the coarsening process, which would be expected in a system with a nonzero atomic diffusion.

Finally, it appears that the shearing of an initially amorphous one-component system constitutes a reproducible way to obtain a nanocrystalline state, which was sometimes taken in the past as a possible model of an amorphous system. It will be interesting to study such a state for its structural, vibrational, and rheological properties, that should be intermediate between those of a glass and of a perfect crystal.

ACKNOWLEDGMENTS

We thank A. Tanguy for useful discussions. Financial support from ANR project SLLOCDYN is acknowledged. The simulations were performed with the classical molecular dynamics package LAMMPS developed by Sandia National Laboratories [32].

[1] P. G. Debenedetti, *Metastable Liquids—Concepts and Principles* (Princeton University Press, Princeton, NJ, 1996).
[2] K. F. Kelton, in *Crystal Nucleation in Liquids and Glasses*, edited by H. Ehrenreich and D. Turnbull (Academic, London, 1991), Vol. 45.
[3] J.-L. Barrat and J.-P. Hansen, *Basic Concepts for Simple and Complex Liquids* (Cambridge University Press, Cambridge, UK, 2003).
[4] P. M. Chaikin and T. C. Lubensky, *Principles of Condensed Matter Physics* (Cambridge University Press, Cambridge, UK, 1995).
[5] *Phase Transitions and Critical Phenomena*, edited by C. Domb and J. L. Lebowitz (Academic, London, 1983), Vol. 8.
[6] R. P. Sear, J. Phys.: Condens. Matter **19**, 033101 (2007).
[7] P. Rein ten Wolde, M. J. Ruiz-Montero, and D. Frenkel, J. Chem. Phys. **104**, 9932 (1996).
[8] J.-X. Yang, H. Gould, W. Klein, and R. D. Mountain, J. Chem. Phys. **93**, 711 (1990).
[9] F. Trudu, D. Donadio, and M. Parrinello, Phys. Rev. Lett. **97**, 105701 (2006).
[10] M. Pluta and A. Galeski, Biomacromolecules **8**, 1836 (2007).
[11] S. Naudy and R. Fulchiron, J. Polym. Sci., Part B: Polym. Phys. **45**, 2982 (2007).
[12] C. Duplay, B. Monasse, J.-M. Haudin, and J.-L. Costa, Polym. Int. **48**, 320 (1999); J. Mater. Sci. **35**, 6093 (2000).
[13] D. Lellinger, G. Floudas, and I. Alig, Polymer **44**, 5759 (2003).
[14] M. L. Wallace and B. Joós, Phys. Rev. Lett. **96**, 025501 (2006).
[15] F. Albano and M. Falk, J. Chem. Phys. **122**, 154508 (2005).
[16] N. Duff and D. J. Lacks, Phys. Rev. E **75**, 031501 (2007).
[17] R. Blaak, S. Auer, D. Frenkel, and H. Löwen, J. Phys.: Condens. Matter **16**, S3873 (2004).
[18] R. Blaak, S. Auer, D. Frenkel, and H. Löwen, Phys. Rev. Lett. **93**, 068303 (2004).
[19] P. Ilg and J.-L. Barrat, Europhys. Lett. **79**, 26001 (2007).
[20] T. K. Haxton and A. J. Liu, Phys. Rev. Lett. **99**, 195701 (2007).
[21] A. Rahman, Phys. Rev. **136**, A405 (1964).
[22] V. Mazzacurati, G. Ruocco, and M. Sampoli, Europhys. Lett. **34**, 681 (1996).
[23] G. Ruocco, F. Sette, R. Di Leonardo, G. Monaco, M. Sampoli, T. Scopigno, and G. Viliani, Phys. Rev. Lett. **84**, 5788 (2000).
[24] A. De Santis, A. Ercoli, and D. Rocca, J. Phys.: Condens.

Matter **14**, L393 (2002).
[25] S. I. Simdyankin, M. Dzugutov, S. N. Taraskin, and S. R. Elliott, J. Non-Cryst. Solids **293–295**, 327 (2001).
[26] P. J. Steinhardt, D. R. Nelson, and M. Ronchetti, Phys. Rev. B **28**, 784 (1983).
[27] S. Butler and P. Harrowell, J. Chem. Phys. **118**, 4115 (2003).
[28] E. Sanz, Ch. Valeriani, D. Frenkel, and M. Dijkstra, Phys. Rev. Lett. **99**, 055501 (2007).
[29] M. D. Rintoul and S. Torquato, J. Chem. Phys. **105**, 9258 (1996).
[30] L. Berthier, J.-L. Barrat, and J. Kurchan, Phys. Rev. E **61**, 5464 (2000).
[31] F. Varnik, L. Bocquet, and J.-L. Barrat, J. Chem. Phys. **120**, 2788 (2004); F. Varnik, L. Bocquet, J.-L. Barrat, and L. Berthier, Phys. Rev. Lett. **90**, 095702 (2003).
[32] http://www.cs.sandia.gov/ sjplimp/lammps.html